Chemical Physics Letters 532 (2012) 72–76

Contents lists available at SciVerse ScienceDirect

Chemical Physics Letters

journal homepage: www.elsevier.com/locate/cplett

Photoluminescence properties of Mn-doped $Zn_xCd_{1-x}S$ nanocrystals synthesized via nucleation-doping strategy

Wei Xu [a,b], Xiangdong Meng [c], Wenyu Ji [a], Pengtao Jing [a], Jinju Zheng [a], Xueyan Liu [a], Jialong Zhao [a,*], Haibo Li [c,*]

[a] State Key Laboratory of Luminescence and Applications, Changchun Institute of Optics, Fine Mechanics and Physics, Chinese Academy of Sciences, 3888 Eastern South Lake Road, Changchun 130033, China
[b] Graduate School of Chinese Academy of Sciences, Beijing 100039, China
[c] Key Laboratory of Functional Materials Physics and Chemistry of the Ministry of Education, Jilin Normal University, Siping 136000, China

ARTICLE INFO

Article history:
Received 30 November 2011
In final form 1 February 2012
Available online 8 February 2012

ABSTRACT

Optical properties of Mn-doped $Zn_xCd_{1-x}S$ nanocrystals were studied by steady-state and time-resolved photoluminescence (PL) spectroscopy. The doped nanocrystals with PL quantum yield up to 29% were synthesized by growing a thin ZnS layer on the MnS core and then growing a CdS layer with different thicknesses using nucleation-doping strategy. The absorption band edge of $Zn_xCd_{1-x}S$ nanocrystals was tuned from 425 to 475 nm by growing the CdS layer with various thicknesses under different Zn/Cd molar ratios to vary the composition. The PL band of Mn-doped nanocrystals was found to originate from emissions of Mn^{2+} ions and defect states.

1. Introduction

Transition-metal ions doped semiconductor nanocrystals (NCs) as a new kind of luminescent nanomaterials have attracted much attention in the past two decades due to their promising applications in light-emitting devices [1,2], biological imaging [3,4], and spin-based electronics [5]. Among semiconductor materials, ZnS, ZnSe, and CdS are particularly suitable to be luminescent hosts for a very large variety of dopants due to their wide band gap energies. For example, transition metal ions such as Mn^{2+} have been successfully doped into ZnS, CdS, and ZnSe NC hosts, exhibiting size- and shape-controlled NC structures with highly efficient photoluminescence (PL) [6–21]. The efficient PL of dopant Mn ions is considered to come from rapid energy transfer from the NC hosts to the dopants under excitation of the doped NCs whose band gap can be tuned with varying the NC size. It is known that the band gap of ternary NCs such as $Zn_xCd_{1-x}S$ and ZnS_xSe_{1-x} can be tuned with varying not only the NC size but also the composition [22,23]. Therefore, the ternary NCs can also provide more suitable hosts for the doping of Mn ions. To date, only a few reports about synthesis of $Zn_xCd_{1-x}S$:Mn quantum dots (QDs) have been given [24–27].

In order to obtain highly efficient PL from Mn ions doped in $Zn_xCd_{1-x}S$ NCs, the dopant ions in the host must be controlled to be far away from nonradiative recombination centers on the surface of NCs. Peng's group reported an effective synthesis route of radial-position-controlled doping into NCs by the growth of a ZnSe shell on the MnSe core using nucleation-doping strategy, resulting in an improvement in the PL quantum yield (QY) of Mn^{2+} ions in ZnSe:Mn/ZnSe QDs and photo/thermal stability of the dots [28–30]. Recently we studied PL properties of Mn ions from the MnS/ZnS core/shell NCs with a PL QY of about 40% synthesized by the strategy [31,32]. The highly efficient PL is considered to come from the emission of Mn ions in ZnS:Mn/ZnS QDs. More recently, Gao group prepared CdS:Mn/CdS QDs by the growth of a CdS shell on the MnS core using the same method [33]. However, in contrast to the yellow emission of isolated Mn ions in the ZnS and ZnSe NC hosts, they observed a broad red emission of Mn ions. Generally, the growth of a CdS shell on the MnS core should result in formation of the interface defects because of the large lattice mismatch of 12% between them. Fortunately, the lattice mismatch between MnS and ZnS and that between ZnS and CdS are only 5% and 7%, respectively, which is much smaller than that between MnS and CdS. Therefore, it is feasible to design a new structure of MnS/ZnS/CdS for synthesizing $Zn_xCd_{1-x}S$:Mn NCs using nucleation-doping strategy.

In this Letter, we report structural and PL properties of Mn-doped $Zn_xCd_{1-x}S$ NCs. The doped NCs with a designed structure of MnS/ZnS/CdS were synthesized by growing a thin ZnS layer on the MnS core as an interface buffer layer and then growing a CdS shell using nucleation-doping strategy. The resulting NCs were characterized by using UV–visible absorption, PL and excitation spectra, X-ray diffraction (XRD) spectroscopy, and transmission

* Corresponding authors.
E-mail addresses: zhaojl@ciomp.ac.cn (J. Zhao), lihaibo@jlnu.edu.cn (H. Li).

0009-2614/$ - see front matter © 2012 Elsevier B.V. All rights reserved.
doi:10.1016/j.cplett.2012.02.001

electron microscopy (TEM). Further, the PL decay kinetics was measured for understanding the origin of the PL band in the Mn-doped NCs.

2. Experimental section

2.1. NC synthesis

2.1.1. Chemicals

Zinc stearate ($ZnSt_2$, 12.5–14% ZnO), stearic acid (SA, 95%), and cadmium oxide (CdO, 99.99%) were purchased from Alpha Aesar. 1-Octadecene (ODE, 90%), oleyamine (OLA, 70%) and oleic acid (OA, 90%) were purchased from Aldrich. Sulfur powders (99.99%) and manganese chloride ($MnCl_2$) were purchased from Shenyang Xinhe Chemical Reagent Company. All chemicals were used without further purification.

2.1.2. Synthesis

The procedure used to synthesize the MnS/ZnS/CdS core/shell NCs was similar to that described in the literatures [31,32]. Octadecene sulfur (ODES) solution was prepared by adding 0.039 g of sulfur and 0.6 mL oeylamine into 3 mL of octadecene (ODE) with heating to clear and holding the solution at 100 °C. The zinc precursor solution was prepared by dissolving 0.1 g of $ZnSt_2$ into 1 mL of ODE with heating to colorless. The cadmium precursor was prepared by a mixture 0.2584 g of CdO, 2 mL of oleic acid and 4 mL of ODE was heated to 180 °C in a 25 mL three-neck flask under argon until the solution turned to clear, and then the additional 7.5 mL of ODE was dissolved to make the concentration of $CdOA_2$ as 0.1 g/mL.

For a typical synthesis of MnS/ZnS/CdS NCs, 12 mL of ODE and 0.03 g of $MnSt_2$ (prepared as Refs. [31,32]) was loaded into a 50 mL three-necked flask and degassed at 110 °C for 15 min by bubbling with argon. The temperature was then raised to 260 °C and 3.6 mL of ODES solution was swiftly injected into the reaction flask. The reaction temperature was swiftly cooled to 150 °C and 1 mL of $ZnSt_2$ solution was added into the reaction flask and then increased to 260 °C and maintained at that temperature for 20 min for ZnS overcoating as well as the Mn^{2+} diffusion. The cadmium precursor solution (1 mL) was added dropwise into the reaction flask at 260 °C and maintained for 5 min, the obtained NCs referred to as sample A. To obtain sample B, the additional $CdOA_2$ solution (1 mL) was injected at 260 °C with 5 min intervals. For samples C and D the total amount of $CdOA_2$ solution was 4 and 6 mL, based on sample B, the remaining $CdOA_2$ solution was injected by adding 2 mL with 10 min intervals for one and two more times, respectively. Finally, the reaction was cooled to room temperature, and the MnS/ZnS/CdS NCs were precipitated using acetone.

2.2. Measurements

The absorption spectra were recorded on a UV-3101PC UV–Vis-NIR scanning spectrophotometer (Shimadzu). Fluorescence and excitation spectra were recorded by a Hitachi F-4500 spectrophotometer. XRD patterns were collected on a Rigaku XRD spectrometer. TEM and high resolution (HR) TEM images were recorded in a Philips TECNAI G2 operated at an accelerating voltage of 200 kV. Energy-Dispersive X-ray Spectroscopy (EDX) was used for the elemental analysis of the inorganic NCs using GENESIS 2000 XMS 60S scanning electron microscope equipped with a field emission gun and operated at 10 kV. In the measurements of fluorescence dynamics, a 355 nm laser generated from a pulsed neodymium doped yttrium aluminum garnet (Nd:YAG) laser combined with a third harmonic generator was used as an excitation light. A Spex 1403 spectrometer and a boxcar integrator were used to record the fluorescence dynamics.

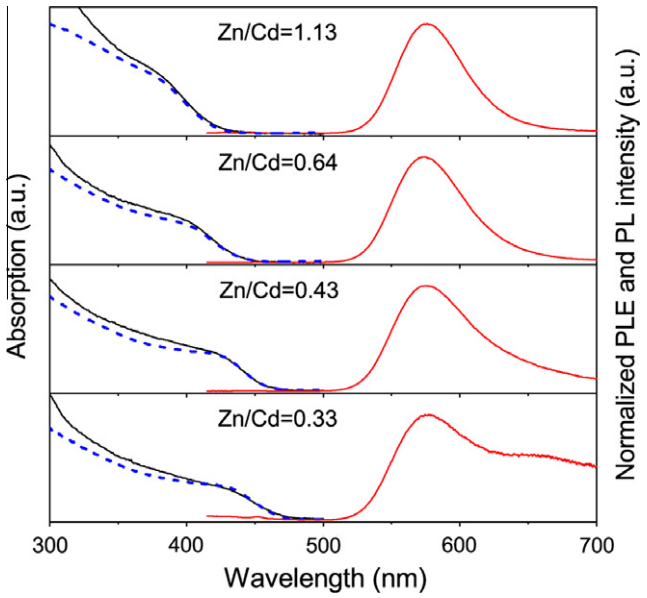

Figure 1. UV–visible absorption (black solid lines), PL (red solid lines) and PLE spectra (blue dashed lines) of MnS/ZnS/CdS core/shell NCs with various Zn/Cd molar ratios as given in the figure. The excitation wavelength is 400 nm. (For interpretation of the references to color in this figure legend, the reader is referred to the web version of this article.)

The PL QY of the MnS/ZnS/CdS NCs was measured following the procedure reported by Pradhan et al. [29]. The PL QY was determined and calibrated by comparing those of dilute yellow-emitting CdSe QDs in hexane whose PL QY keeps the same under excitation wavelengths of 400 (the excitation wavelength of the MnS/ZnS/CdS NCs) and 490 nm (the excitation wavelength of Rhodamine 6G)

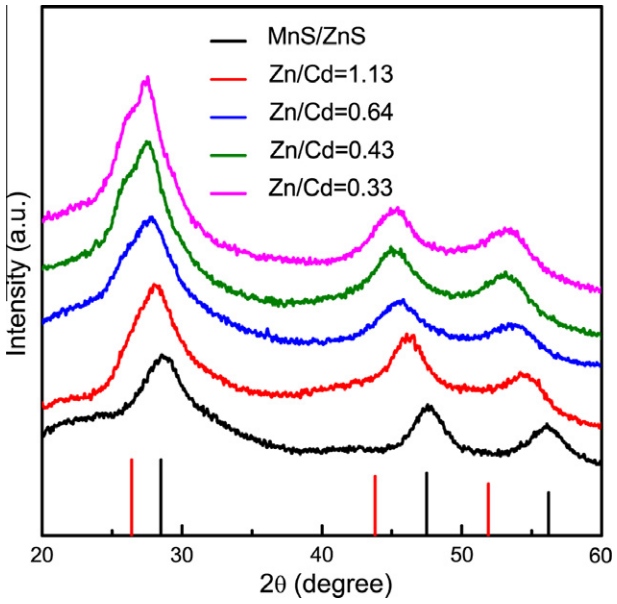

Figure 2. XRD patterns of MnS/ZnS/CdS core/shell NCs with Zn/Cd ratios of 1.13 (red line), 0.64 (blue line), 0.43 (olive line), and 0.33 (pink line) from top to bottom. The black line represents the XRD pattern of MnS/ZnS core NCs. The standard diffraction patterns of zinc-blende bulk ZnS (JCPDS No. 05-0566) and CdS (JCPDS No. 65-2887) are also shown in the figure by vertical black and red bars. (For interpretation of the references to color in this figure legend, the reader is referred to the web version of this article.)

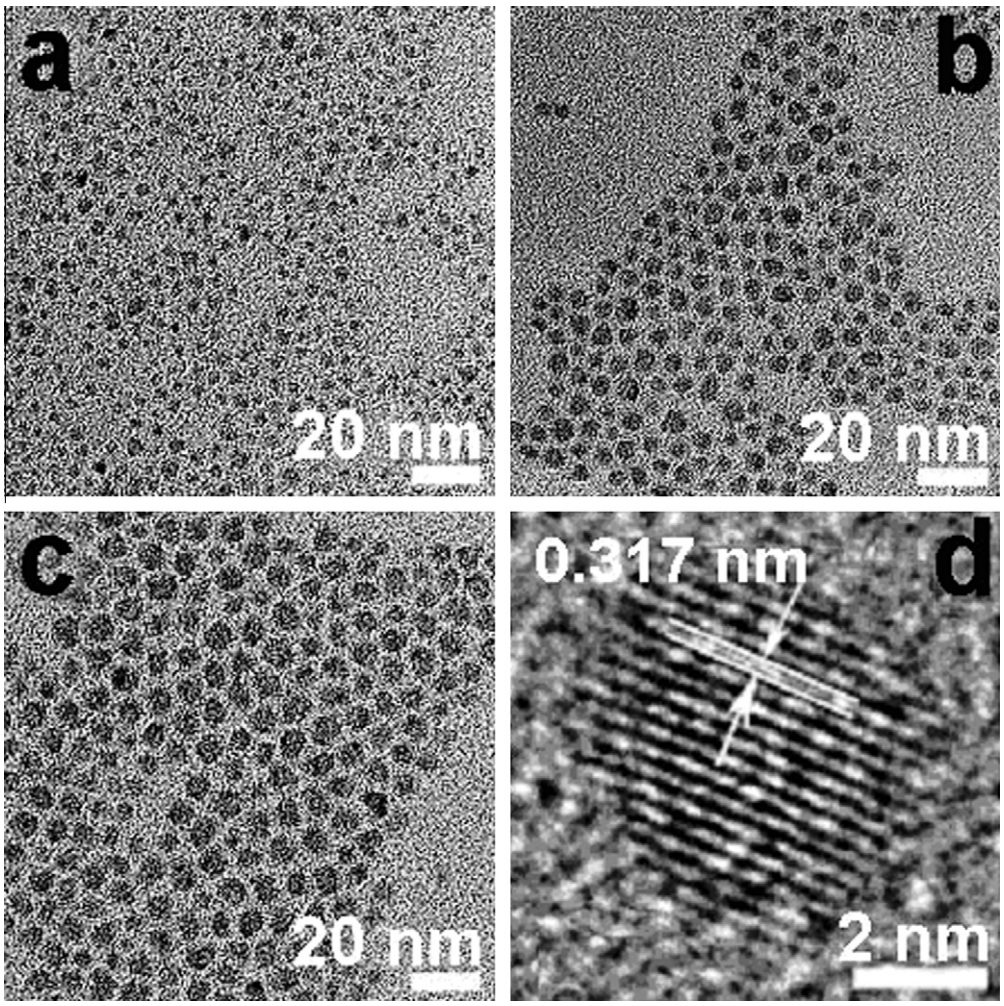

Figure 3. Representative TEM images of MnS/ZnS (a) and MnS/ZnS/CdS NCs core/shell NCs with Zn/Cd radios of 0.64 (b) and 0.33 (c). A HRTEM image of MnS/ZnS/CdS NCs with a Zn/Cd ratio of 0.64 is shown in (d).

and Rhodamine 6G dye with a PL QY of 95% in ethanol. The error of the measurement was estimated to be smaller than 10% of the obtained values.

3. Results and discussion

Figure 1 shows UV–visible absorption, PL and PL excitation (PLE) spectra of the MnS/ZnS/CdS core/shell NCs with different CdS shell thicknesses. The MnS cores with about two monolayers (MLs) of ZnS shell were prepared by the procedure that we used previously [31,32]. The CdS shells with various thicknesses were grown on the MnS/ZnS particles by adding different contents of cadmium precursor during injection synthetic process. The molar ratio of Zn to Cd was estimated to be 1.13, 0.64, 0.43, and 0.33 by EDX, and their corresponding composition x in the NCs was determined to be 0.53, 0.39, 0.30, and 0.25, respectively. As seen in Figure 1, the obtained MnS/ZnS/CdS NCs with a thin CdS shell exhibit a well-resolved excitonic absorption band edge at 425 nm. The absorption band gradually shifts to longer wavelength as the CdS layer grows thicker. On the other hand, a bright yellow PL band peaked at 575 nm was observed when the CdS shell was grown on the MnS/ZnS particles. The peak wavelength is almost kept constant when the optical absorption band edge of MnS/ZnS/CdS NCs changes from 425 to 475 nm. In general, the orange PL band peaked at about 585 nm is considered to originate from a typical emission of Mn^{2+} ions due to their $^4T_1$ to $^6A_1$ transition in ZnS NCs [8–14]. Mn doped CdS NCs exhibited a strong PL band with a peak wavelength near 580 nm [15–19]. The PL of Mn-doped ZnSe NCs were observed from about 565 to 610 nm, which was related to the crystal field splitting effect of the d-orbitals or the cation precursor effect [29]. These observations mean that the different peak wavelength of the Mn doped NCs is related to the lattice environment of Mn ions in the host. Further, it is noted that the PLE spectra of the yellow emission in the NCs are well consistent with the absorption onset of the MnS/ZnS/CdS NC host, indicating that the PL comes from the Mn ions in the photoexcited MnS/ZnS/CdS host through an energy transfer process. In addition, the full width at half maximum (FWHM) of the PL band of MnS/ZnS/CdS NCs with increasing the CdS shell thickness slightly broadens when the Zn/Cd molar ratio changes from 1.13 to 0.43. An emission shoulder is observed at the longer wavelength side of the PL band when the Zn/Cd molar ratio decreases to 0.33. The narrow PL FWHM of the NCs with a large Zn/Cd molar ratio is well consistent with that of highly luminescent ZnS:Mn [8–14], CdS:Mn [15–19], and ZnSe:Mn [20,21]. On the other hand, the PL QY of the NCs was found to significantly increase from 15% to 29 % when the Zn/Cd ratio changed from 1.13 to 0.64, perhaps indicating the significant improvement of the PL QY for MnS/ZnS/CdS NCs by a thick CdS shell. The similar PL enhancement with increasing shell

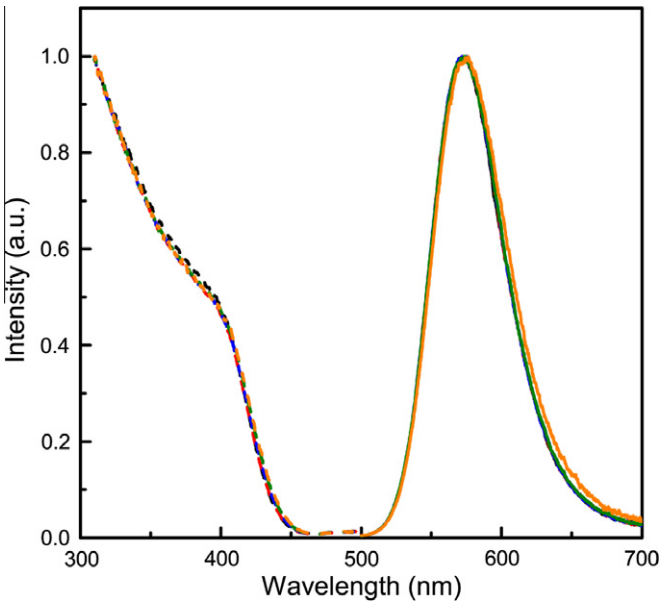

Figure 4. Normalized PL (right) and PLE spectra (left) of Mn-doped $Zn_xCd_{1-x}S$ NCs with a Zn/Cd ratio of 0.64 at different excitation or emission wavelengths as shown in this figure by solid (dashed) black, red, blue, olive, and orange lines, respectively. (For interpretation of the references to color in this figure legend, the reader is referred to the web version of this article.)

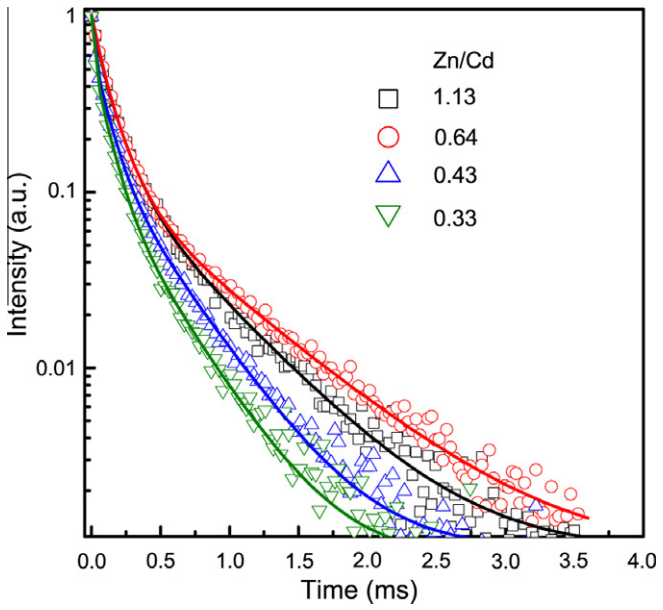

Figure 5. Decay curves of the PL band at 580 nm in Mn-doped $Zn_xCd_{1-x}S$ NCs with Zn/Cd ratios of 1.13, 0.64, 0.43, and 0.33 recorded at room temperature. The solid lines represent fitting curves.

thickness was also observed in MnS/Mn:ZnS QDs [31,32]. The PL QY of the MnS/ZnS/CdS NCs drops rapidly from 29% to 7% when the Zn/Cd molar ratio decreases to 0.33, perhaps resulting from formation of some nonradiative recombination centers in the NCs.

The XRD patterns of Mn-doped MnS/ZnS/CdS core/shell NCs with Zn/Cd molar ratios of 1.13, 0.64, 0.43, and 0.33 are shown in Figure 2. The XRD data confirm that the NCs have the cubic zinc-blende structure. Three diffraction peaks of MnS cores located at 27.4°, 45.6°, and 54.0°, corresponding to the (111), (220), and (311) planes of zinc-blende phase MnS (JCPDS No. 40-1288), respectively, were shown in our previous results [32]. As seen in Figure 2, the peaks of the MnS/ZnS particles are close to the standard positions of zinc-blende ZnS (JCPDS No. 05-0566). The strongest peak shifted to the low angle from 28.62° to 27.37° when a CdS shell with different thickness was grown on the surface of MnS/ZnS particles. It is noted that the peaks of the MnS/ZnS/CdS NCs are located between the standard JCPDS No. 05-0566 (for cubic ZnS) and JCPDS No.65-2887 (for cubic CdS) which are shown in Figure 2 by vertical black and red bars on the bottom of the *Y*-axis. The dependence of continuous shifting of the diffraction peaks on the composition indicates the formation of $Zn_xCd_{1-x}S$ alloyed NCs rather than their separate nucleation or phase formation. In addition, no effect of the doping of Mn^{2+} ions on the XRD pattern was observed in alloyed NCs.

Figure 3a–c shows typical TEM images of MnS/ZnS particles, MnS/ZnS/CdS NCs with Zn/Cd ratios of 0.64 and 0.33, respectively. The MnS/ZnS particles have an average diameter of 3.5 nm. The ternary MnS/ZnS/CdS NCs are nearly spherical and well monodispersed. The average diameters of the NCs with Zn/Cd ratios 0.64 and 0.33 were determined to be 4.8 and 7.1 nm, respectively, which indicated that the growth of the 2.0 and 5.5 ML thick CdS shells on the MnS/ZnS particles. As seen in Figure 3d, a HRTEM image of Mn-doped MnS/ZnS/CdS NCs with a Zn/Cd ratio of 0.64 indicates that the lattice spacing of 0.317 nm probably corresponds to the (111) plane of the zinc-blende phase of the $Zn_xCd_{1-x}S$ alloy NCs, which is slightly larger than the value for the (111) d spacing measured as 0.312 nm of the MnS/ZnS core/shell NCs in the literature [31]. On the other hand, on the basis of the HRTEM image of the NCs, the distinguishable lattice plane reveals that as-synthesized MnS/ZnS/CdS NCs are highly crystalline and any crystal boundary among the MnS core, ZnS shell, and CdS shell is not observed, indicating formation of Mn-doped $Zn_xCd_{1-x}S$ NCs.

The site-selective optical spectroscopy is a good tool to study the origin and local environment of emission centers in semiconductor hosts. The normalized PL spectra at different excitation wavelengths and PLE spectra at different emission wavelengths for Mn-doped $Zn_xCd_{1-x}S$ NCs with a Zn/Cd ratio of 0.64 are shown in Figure 4. The emission wavelength of Mn ions in the ZnS, CdS, ZnSe hosts is very sensitive to the symmetry of the crystalline field for Mn ions in different radical positions of NCs [8–21,28–30]. As seen in Figure 4, the peak wavelength of the PL band for $Zn_xCd_{1-x}S$ NCs with a Zn/Cd ratio of 0.64 at excitation wavelengths of 325, 350, 375, 400, and 425 nm is kept constant. On the other hand, the normalized PLE spectra are almost the same when different emission positions at 540, 560, 580, 600 and 620 nm are detected. Therefore, no significant change in these PL and PLE spectra clearly suggests that the PL in MnS/ZnS/CdS QDs comes from the emission of Mn ions in $Zn_xCd_{1-x}S$ NCs and not from the emission of Mn ions doped in isolated ZnS or CdS NC hosts, respectively. In addition, no local environment effect on the PL emission of Mn ions was observed.

Figure 5 shows PL decay curves of the Mn-doped $Zn_xCd_{1-x}S$ NCs with Zn/Cd ratios of 1.13, 0.64, 0.43, and 0.33 at room temperature. For the four NC samples, the emission detected at 580 nm exhibited a nonexponential decay which was fitted by a tri-exponential function, $I(t) = A_1\exp(-t/\tau_1) + A_2\exp(-t/\tau_2) + A_3\exp(-t/\tau_3)$, where τ_1, τ_2, and τ_3 are the time constants, and A_1, A_2, and A_3 are the normalized amplitudes of the components, respectively [10,11,35,36]. The decay time constants of the three components were on the scale of 350–665 μs, 99–144 μs, and tens of μs, respectively. It is known that the origins of the decays in Mn-doped ZnS and CdS NCs have been extensively studied. The slowest component in the range of ms was attributed to the emission of the single isolated Mn^{2+} ions in a cubic site [10,11,16,18]. The fastest decay component with the time constants of tens of μs might have a contribution from non-radiative recombination centers or be related to the emission of surface defects [10,11,16,18]. Therefore,

the slowest and medium decay components in our experiment are attributed to the emissions of Mn^{2+} ions in the Mn-doped $Zn_xCd_{1-x}S$ NCs. The fastest decay component with the time constant of tens of μs might come from the emission of defect states in the NCs.

The experimental results above have already demonstrated that Mn^{2+} ions in $Zn_xCd_{1-x}S$ NCs prepared by nucleation-doping strategy exhibit highly efficient PL emission, compared with Mn^{2+} ions in $Zn_xCd_{1-x}S$ NCs obtained by growth-doping method [24–27]. The growth process of the $Zn_xCd_{1-x}S$ NCs can be understood on the basis of the MnS/ZnS/CdS structure as follows [28–32,34]: First, small-sized MnS cores were formed under the cationic precursor $MnSt_2$ and excess S precursor. Second, a thin ZnS shell was grown on the MnS core under 260 °C. During the growth of the ZnS layer, amount of Mn^{2+} ions diffused into the ZnS layer. Third, during the growth of a CdS shell with different thickness on the MnS/ZnS particles at a high temperature of 200–260 °C, the $Zn_xCd_{1-x}S$ alloy layer formed during the growth of the CdS layer. Mn ions would diffuse into the $Zn_xCd_{1-x}S$ alloy layer under the high temperature. The composition of the Mn ions doped $Zn_xCd_{1-x}S$ alloy layers was controlled by varying the thickness of the CdS layer.

4. Conclusions

In summary, we have successfully synthesized highly efficient luminescent Mn-doped $Zn_xCd_{1-x}S$ alloy NCs based on the MnS/ZnS/CdS structure using nucleation-doping strategy. The Mn-doped NCs with a PL QY up to 29% was achieved by the growth of a CdS layer on the MnS/ZnS particles. The absorption band edge of the Mn-doped NCs was tuned from 425 to 475 nm with varying the Zn/Cd ratio. It was found that the PL band in the NCs was composed of emissions of Mn ions and defect states. Therefore, it is expected that the PL QY of Mn-doped $Zn_xCd_{1-x}S$ NCs can be further improved by the growth of a ZnS shell on the surface of the NCs to decrease the nonradiative centers.

Acknowledgments

This work was supported by the program of CAS Hundred Talents, the National Natural Science Foundation of China (No. 10874179, 60976049 and 51102227). We thank Professor Yasuaki Masumoto for his helpful discussion.

References

[1] H. Yang, P.H. Holloway, B.B. Ratna, J. Appl. Phys. 93 (2003) 586.
[2] V. Wood, J.E. Halpert, M.J. Panzer, M.G. Bawendi, B. Vladimir, Nano Lett. 9 (2009) 2367.
[3] J.Q. Zhuang, X.D. Zhang, G. Wang, D.M. Li, W.S. Yang, T.J. Li, J. Mater. Chem. 13 (2003) 1853.
[4] R. Thakar, Y.C. Chen, P.T. Snee, Nano Lett. 7 (2007) 3429.
[5] R. Beaulac, P.I. Archer, S.T. Ochsenbein, D.R. Gamelin, Adv. Funct. Mater. 18 (2008) 3873.
[6] S.C. Erwin, L. Zu, M.I. Haftel, A.L. Efros, T.A. Kennedy, D.J. Norris, Nature 436 (2005) 91.
[7] D.J. Norris, A.L. Efros, S.C. Erwin, Science 319 (2008) 1776.
[8] R.N. Bhargava, D. Gallagher, X. Hong, A. Nurmikko, Phys. Rev. Lett. 72 (1994) 416.
[9] R.N. Bhargava, J. Lumin. 70 (1996) 85.
[10] A.A. Bol, A. Meijerink, Phys. Rev. B 58 (1998) R15997.
[11] B.A. Smith, J.Z. Zhang, A. Joly, J. Liu, Phys. Rev. B 62 (2000) 2021.
[12] L.X. Cao, J.H. Zhang, S.L. Ren, S.H. Huang, Appl. Phys. Lett. 80 (2002) 4300.
[13] Z.W. Quan, Z.L. Wang, P.P. Yang, J. Lin, J.Y. Fang, Inorg. Chem. 46 (2007) 1354.
[14] Y.A. Yang, O. Chen, A. Angerhofer, Y.C. Cao, J. Am. Chem. Soc. 128 (2006) 12428.
[15] M.A. Chamarro et al., J. Cryst. Growth 159 (1996) 853.
[16] Y. Kanemitsu, H. Matsubara, C.W. White, Appl. Phys. Lett. 81 (2002) 535.
[17] H. Yang, P.H. Holloway, Adv. Funct. Mater. 14 (2004) 152.
[18] A. Ishizumi, Y. Kanemitsu, Adv. Mater. 18 (2006) 1083.
[19] A. Nag et al., J. Phys. Chem. C 114 (2010) 18323.
[20] D.J. Norris, N. Yao, F.T. Charnock, T.A. Kennedy, Nano Lett. 1 (2001) 3.
[21] R.S. Zeng, M. Rutherford, R.G. Xie, B.S. Zou, X.G. Peng, Chem. Mater. 22 (2010) 2107.
[22] X.H. Zhong, Y.Y. Feng, W. Knoll, M.Y. Han, J. Am. Chem. Soc. 125 (2003) 13559.
[23] X.H. Zhong, M.Y. Han, Z.L. Dong, T.J. White, W. Knoll, J. Am. Chem. Soc. 125 (2003) 8589.
[24] J.U. Kim, M.H. Lee, H. Yang, Nanotechnology 19 (2008) 465605.
[25] Z.Q. Chen et al., Chem. Phys. Lett. 488 (2010) 73.
[26] N.S. Karan, D.D. Sarma, R.M. Kadam, N. Pradhan, J. Phys. Chem. Lett. 1 (2010) 2863.
[27] A. Nag, S. Chakraborty, D.D. Sarma, J. Am. Chem. Soc. 130 (2008) 10605.
[28] N. Pradhan, D. Goorskey, J. Thessing, X.G. Peng, J. Am. Chem. Soc. 127 (2005) 17586.
[29] N. Pradhan, X.G. Peng, J. Am. Chem. Soc. 129 (2007) 3339.
[30] N. Pradhan, D.M. Battaglia, Y.C. Liu, X.G. Peng, Nano Lett. 7 (2007) 312.
[31] J.J. Zheng et al., J. Phys. Chem. C 113 (2009) 16969.
[32] J.J. Zheng et al., J. Phys. Chem. C 114 (2010) 15331.
[33] T.S. Zuo, Z.P. Sun, Y.L. Zhao, X.M. Jiang, X.Y. Gao, J. Am. Chem. Soc. 132 (2010) 6618.
[34] R.S. Zeng, T.T. Zhang, G.Z. Dai, B.S. Zou, J. Phys. Chem. C 115 (2011) 3005.
[35] L. Qian, D. Bera, P. Holloway, Appl. Phys. Lett. 92 (2008) 093103.
[36] C.L. Gan, Y.P. Zhang, D. Battaglia, X.G. Peng, M. Xiao, Appl. Phys. Lett. 92 (2008) 241111.